Open access • Journal Article • DOI:10.1103/PHYSREVLETT.105.066103

Structural and Phase Changes in Amorphous Solid Water Films Revealed by Positron Beam Spectroscopy — Source link

Yichu Wu, Yichu Wu, Alexis Kallis, J Jiang ...+1 more authors

Institutions: Wuhan University, University of Bath

Published on: 05 Aug 2010 - Physical Review Letters (American Physical Society)

Topics: Positron annihilation spectroscopy, Amorphous solid, Crystallization, Positron and Positronium

Structural and phase changes in amorphous solid water films revealed by positron beam spectroscopy

Y.C. Wu[1,2], A. Kallis[1], J. Jiang[2] and P.G. Coleman[1]

[1]Department of Physics, University of Bath, Bath BA2 7AY, UK

[2] Department of Physics, Wuhan University, Wuhan 430072, P.R.China

The evolution and annealing of pores in, and the crystallization of, vapor-deposited films of Amorphous Solid Water (ASW) have been studied using variable energy positron annihilation spectroscopy for temperatures in the range 50-150K. Both positron and positronium annihilation provide an insight to the nature of the grown-in pores and their evolution with temperature. Crystallization of the films was observed at just below 140K, in agreement with earlier studies, with the topmost 80nm undergoing a transition consistent with crystallization at 90-100K.

PACS numbers: 61.43.Er, 64.70.dg, 68.55.-a, 78.70.Bj

The abundance and many unusual properties of ice, the solid phase of water, have made it the subject of a large number of experimental investigations over many decades [1]. While on Earth most solid water has a hexagonal crystalline form, amorphous solid water (ASW) is the most abundant phase of water elsewhere in the galaxy. The physical properties of ASW are strongly influenced by growth conditions [2] – for example, water vapor deposited on a cold (<130 K) substrate forms a noncrystalline, thermodynamically unstable material known as low density ASW, which is thus believed to be a major component of comets, planetary rings, and interstellar clouds. ASW is also a metastable extension of liquid water and as such is a model system for studying deeply supercooled liquids. Consequently, the physical and chemical properties of ASW, which are intimately related to its morphology, are of considerable interest to physical chemists, astrophysicists, planetary scientists, and cryobiologists [3]. While this kinetically ‘‘frozen’’ substance can persist for extended periods at temperatures below about 130 K, above 135 K ASW transforms to a stable crystal phase, cubic ice, on a laboratory time scale [4]. There remains controversy about the fundamental properties of ice including crystallization and glass transformation temperatures [5], and whether crystallization is initiated in the bulk [6] or at the surface [7]. Problems also exist with the study of pores in ice films; studies of gas adsorption on vapor-deposited ASW [8-10] have revealed that the amount of gas uptake is consistent with microporosity (pore width < 2 nm), and large specific surface areas of up to hundreds of m^2g^{-1}. However, when pores become too small, or pore structures have no connection to the surface, they may not be detected.

Variable-Energy Positron Annihilation Spectroscopy (VEPAS) is well suited to the non-destructive study of phase transitions and pore structures in ASW films. While positrons are sensitive to structural changes, both positrons and positronium (Ps), the positron-electron bound state, are highly sensitive to open volume in a material. Their sensitivity ranges from monovacancies (positrons) to voids to pores of $\sim 10^1$ nm in diameter (Ps). In the last case, the probability of ortho-Ps (the spin triplet state) decaying into three gamma photons depends on the size distribution and interconnectivity of the pores. VEPAS has been successfully applied to the study of

porous films [11,12]. In VEPAS a beam of mono-energetic positrons is implanted into a thin-film ASW sample in a high-vacuum environment with a range of chosen mean depths [13] so that it non-invasively depth profiles its structural properties. The only previous reports of its application to ice films are those of Eldrup et al. [14,15] who studied the probability of formation and escape of Ps at very low (~eV) incident positron energies, and measured the Ps diffusion coefficients in crystalline and amorphous ice (0.2 and 10^{-3} cm^2s^{-1}, respectively) using positrons with incident energy below 4.5keV. To date there has been no VEPAS study of the structure of, and evolution of pores in, ASW, and this is the focus of the research presented here.

The Doppler broadening parameters *S* and *W*, linked to the annihilation of positrons by low- and high-momentum electrons, respectively [13], and *R*, the ratio of 3γ:2γ annihilations, reflecting the probability of Ps decaying as ortho-Ps, have been measured as a function of incident positron energy *E* from 0.25 to 30 keV (corresponding to mean depths of up to ~ 10 μm) and sample temperatures from 50 to 150K.

The experiments were performed in a magnetic-transport positron beam system [16] with base pressure ~ 10^{-6} Pa. ASW films were grown from a diffuse water vapor background flux on to a copper cylinder block, cooled by a closed-cycle He cryostat to 50K. The water vapor was leaked into the sample chamber via a needle valve from a side chamber containing deionized water initially subjected to several freeze–pump–thaw cycles. The sample temperature was controlled by a calibrated silicon-diode sensor and measured by a *K*-type thermocouple clamped on the sample holder to an accuracy of ±1 K. The ASW samples were grown at rates between 5 and 200nm min^{-1} and their thicknesses were thereby controllable. The upper temperature limit for VEPAS measurements, 150K, was that above which the ice film sublimed.

Annihilation gamma energy spectra were recorded for each incident positron energy *E* by a high-purity Ge detector system. The spectra included (a) the 511keV photopeak, from which the Doppler broadening parameters *S* (sharpness, defined by the fraction of the peak in a predefined central region) and *W* (wing, the fraction of the peak in the two predefined wing regions) were obtained, and (b) a narrow valley

region between about 475-505 keV, from which the 3γ:2γ parameter R (the ratio of valley to photopeak counts) was deduced. The parameter F, which is proportional to the probability that the implanted positrons will be annihilated as Ps, was then calculated using $F = (R - R_0)/(R_1 - R_0)$, where R_0 is the value of R when no Ps is formed (e.g., in copper for E = 30 keV) and R_1 is the maximum value of R measured in the studies featured here (at E = 0.5 keV). 10^6 events were typically recorded in the annihilation photopeak for each E. $S(E)$, $W(E)$ and $F(E)$ were fitted as necessary using the standard code VEPFIT [17].

When monoenergetic positrons are implanted into a porous ASW film, they are quickly thermalized with a gaussian-derivative depth profile $P(z,E)$ with mean depth $\bar{z}$ for a solid of unit density approximately given by $40E^{1.6}$ nm (E in keV) [13]. Some are annihilated in the ice, while some form Ps, which is trapped in the pores. The larger the pores, the greater the probability that ortho-Ps will survive to decay into 3γ and the larger the parameter F will be. Further, if some pores are interconnected and form an open channel which ends at the surface, this can provide a pathway for ortho-Ps to reach the vacuum above the film. The deeper the Ps is formed the greater the chance that it will be annihilated into 2γ via collision with the channel wall, and the lower the yield of the 3γ annihilation events. By fitting the parameter F measured as a function of E (i.e., probed depth) one can thus estimate the effective Ps diffusion length L_{Ps} and therefore elucidate pore interconnectivity. $F(E) = F_S f_S(E) + F_B(1-f_S(E))$, where F_S and F_B are the parameter values at the surface (i.e., at $E \rightarrow 0$) and in the bulk film, and $f_S(E) = \int P(z,E)\exp(-z/L_{Ps})dz$ is the fraction of implanted positrons which decay as Ps into three gamma photons at or above the surface. This use of ortho-Ps to study pore morphology was reviewed by Weber and Lynn [18]. It is important to note here that, although qualitative information on the evolution of micro- and meso-pores (typically of size <2 and 2-50 nm, respectively) can be gained from the current measurements, quantitative assignment of pore sizes and densities is not possible without resolving a number of experimental issues, as listed by Wang et al. [19]

$F(E)$ at different temperatures for an exemplar ASW film – several microns thick - grown at 50K at a rate of 6nm min^{-1} on a pre-existing crystalline ice film are shown in Fig. 1(a). The mean implantation depth $\bar{z}$ of positrons in a unit-density film is shown on the upper horizontal axis. The non-monotonic behavior of some of the data at low E is associated with the partial non-thermalization of positrons implanted with energies below ~ 1keV. The effective ortho-Ps diffusion lengths obtained by fitting these data (for E > 1 keV) falls from ~ 120nm at low temperatures to a minimum of ~12 nm at 120K, reflecting a decrease in the interconnectivity between pores as the temperature is increased. Fillion et al. [20] reported that compact or nonporous ASW films can be grown at 120K. For $T \geq$ 140K, ortho-Ps diffusion lengths increase again to ~ 40nm, consistent with the larger Ps diffusion coefficient in crystalline ice [15], allowing more Ps atoms to escape into the vacuum (as demonstrated by the higher near-surface F values at these temperatures). It is to be noted that although the diffusion lengths obtained from this fitting procedure may be model-dependent, and are affected by the presence of pores and smaller defects, their relative variation with T is still valid.

In Fig. 1(b) the fitted film F_B values are plotted against sample temperature for the film whose raw data are shown in Fig. 1(a), together with F values for a second film, grown to a depth of ~ 700nm directly on to the copper substrate at 50K at a rate of 5 nm/min. In the first film, which is typical of most ice films grown in this study, F decreases with T, eventually reaching an asymptotic value close to zero, indicative of pore collapse. Above 135K F increases suddenly when the film undergoes crystallization. On recooling the film to 130 and then 50K, F changes only slightly, consistent with the irreversibility of the phase transition. F for the second, thinner film increases from a much lower value for the as-grown film until it meets the values for the thicker film at ~100K. It is postulated, as F is small for closed pores and large for interconnected pores, that in this lower-temperature range closed or part-closed pores are clustering into open or interconnected geometries.

$S(E)$ and fitted film $S(T)$ plots for the 700nm ASW film featured in Fig. 1(b) are shown in Figs. 2(a) and (b), respectively. The parameters are normalized to the value for the copper substrate (whose S value is thus unity). The concentration of defects at the ASW film/Cu interface is considered to be below the detection limit of the technique. In the raw data (Fig. 2(a)) there exist ranges of E (2-5keV) over which the essentially constant S value can be directly attributed to the film, before decreasing towards the copper substrate value at higher E. Fig. 2(b) shows that S is strongly sensitive to the amorphous-to-crystalline phase transition in the vicinity of 135K, which again is seen to be irreversible.

Of special interest in Fig. 2 is the unusual irreversible increase in S in a thin (~ 80nm) surface layer seen at about 90K. This was seen in all samples grown but is more noticeable in this film, where the initial film S value is low.

To investigate this phenomenon further, $S(E)$ is plotted against $W(E)$ for T = 50-150K in Fig. 3. Each 'pure' annihilation state occupies a particular point on this graph; e.g., annihilation in the copper substrate is represented by the point at (1,1) (Cu). Also marked on the graph are the states associated with the ASW film (A), crystalline ice (C), and the surface (S) (the S,W values approached as $E \rightarrow 0$). At low T, the $S(E)$ points lie on a line joining Cu to A. At high T they lie between Cu and C. However, at 90K a change can be seen in the (solid) points corresponding to low E, which turn towards and (at 110K) reach point C. This evidence is consistent with the formation of a crystalline layer in the first few 10's nm from the surface; this may be associated with the formation of crystalline ice clusters or islands, as ice molecules are highly diffusive at the surface. This has been confirmed by recent STM observations of the top surface layers [21,22].

The three main features shown by F for the thin film in Fig. 1(b) are also displayed $S(T)$ in Fig. 2(b): a small increase between 50-90 K, attributed to clustering of pores; a small decrease between 90 and 130 K, attributed to pore collapse; and a sudden irreversible increase above 130 K when the film undergoes crystallization at around 140K. This comparison demonstrates that S is more sensitive to the phase transition and F is more sensitive to the pore structure.

The growth conditions and annealing temperatures strongly influence on the physical properties of ASW film. *S* vs *T* for four films grown at 50K are compared in Fig. 4. In addition to the two films featured in Fig. 1(b), two further films were grown on Cu at 50K to thicknesses of several microns at 7 and 200 nm/min. Fig. 4 shows that S increases with growth rate, a result also observed for *F* (see Fig. 1(b) at low T). This implies that more closed pores were formed when the growth rate was faster, which results in the increase of *S*.

The main results of the work presented here can be summarized as follows.

(i) *Annealing of open/interconnected pores.* The behavior of the Ps fraction *F* is sensitive to the pore structure of the films, suggesting almost complete annealing by 120K. These results can be interpreted in a similar way to a nitrogen adsorption experiment [3] – however, *F* is more sensitive and directly reflects the porosity of ASW films.

(ii) *Annealing of closed pores.* The relative differences in *S* for the different films stems from the differences of size and number of closed pores. *S*(*T*) before the onset of crystallization is similar for all the films studied, again reflecting pore clustering and collapse.

(iii) *Amorphous to crystalline transition.* Both *S* and *F* increase suddenly when the films becomes crystalline between 130-140K. *F* is determined by pore interconnectivity (i.e., predominantly by growth temperature) and is relatively insensitive to other growth conditions, in contrast to *S*, which depends on the closed pore size and density in the ASW films. A slightly (~ 5K) lower crystallization temperature was measured for the ASW film grown on crystalline ice. *S* in crystalline ice films has contributions from para-Ps annihilation, quenched (2γ) ortho-Ps annihilation, and positrons trapped in defects in the crystal lattice, as well as bulk crystalline ice. For the fast-grown sample, many closed pores remained at 130 K, and so *S* shows a small change. In contrast, for the samples grown more slowly, there are far fewer closed pores and so *S* changes more markedly.

(iv) *Formation of thin crystalline surface layer.* An unusual increase in *S* for the near-surface layer (thickness ~ 80nm) between 90-120K was observed, but no

corresponding change in *F* was seen. This is consistent with our conclusion that *S* is much more sensitive to the phase of the ice than is *F*, and with the earlier result [14,15] that Ps diffuses readily through thin layers of crystalline ice. We are led to the conclusion that crystallization takes place in the near-surface layer, which can be attributed to or driven by the reorganization of water molecules and/or the formation of ice islands at the surface.

Finally, preliminary observations of time dependent changes in *F* and *S* via short repeated runs at 50 and 140K holds promise that VEPAS can provide a method for quantifying the energetics of crystallization and near-surface changes associated with molecular mobility.

YCW acknowledges the support of the National Nautural Science Foundation of China under grant no. 10975110. The authors are grateful to Prof. M.A. Alam and Dr. S.B. Dugdale for suggesting this problem to them, and to the China Scholarship Council for providing financial support for YCW during the performance of this research.

[1] P. Jenniskens and D.F. Blake, Science **265**, 753 (1994).

[2] C. Austen Angell , Science **319**, 582 (2008).

[3] K. P. Stevenson, G. A. Kimmel, Z. Dohnalek, R. Scott Smith and B. D. Kay, Science **283**, 1505 (1999).

[4] D. J. Safarik and C. B. Mullins, , J. Phys. Chem. 121, 6003(2004).

[5] J. Cyriac and T. Pradeep, J. Phys. Chem. C 112, 5129-5135(2008).

[6] R. Scott Smith, C. Huang, E.K.L. Wong and B.D. Kay, Surf. Sci. 367, L13 (1996).

[7] E.H.G. Backus, M.L. Grecea, A.W. Kleyn and M. Bonn, Phys. Rev. Lett. 92, 236101 (2004).

[8] U. Raut, M. Famá, B. D. Teolis, and R. A. Baragiola, J. Chem. Phys. 127, 204713 (2007).

[9] R.S. Smith, T. Zubkov, Z. Dohnalek and B.D. Kay, J. Phys. Chem. B 113, 4000 (2009).

[10] P. Ayotte, R.S. Smith, K.P. Stevenson, Z. Dohnalek, G.A. Kimmel and B.D. Kay. J. Geophys. Research - Planets 106, 33387 (2001).

[11] D.W. Gidley, W.E. Frieze, T.L. Dull, A.F. Yee, E.T. Ryan and H.M. Ho, Phys. Rev. B **60**, R5157 (1999).

[12] R. Suzuki, T. Ohdaira, Y. Shioya and T. Ishimaru, Jpn. J. Appl. Phys., **40**, L414 (2001).

[13] *Positron Beams and Their Applications*, P.G. Coleman (ed.), (World Scientific: Singapore, 2000).

[14] M. Eldrup, A. Vehanen, P.J. Schultz and K.G. Lynn, Phys. Rev. Lett. **51**, 2007 (1983).

[15] M. Eldrup, A. Vehanen, P.J. Schultz and K.G. Lynn, Phys. Rev. B **32**, 7048 (1985).

[16] N. B. Chilton and P. G. Coleman, Meas. Sci. Technol. **6**, 53 (1995).

[17] A. van Veen, H. Schut, J. de Vries, R.A. Hakvoort and M.R. IJpma, AIP Conf. Proc. **218**, 171 (1990).

[18] Marc H. Weber and Kelvin G. Lynn, in *Principles and Applications of Positron and Positronium Chemistry*, eds. Y.C. Jean, P.E. Mallon and D.M. Schrader (World Scientific: Singapore, 2003) pp. 167-210.

[19] C.L. Wang, M.H. Weber and K.G. Lynn, J. Appl. Phys. **99**, 113514 (2006).

[20] J.-H. Fillion, L. Amiaud, E. Congiu, F. Dulieu, A. Momeni and J.-L. Lemaire, Phys. Chem. Chem. Phys. **11**, 4396 (2009).

[21] M. Mehlhorn and K. Morgenstern, New J. Phys. **11,** 093015 (2009).

[22] T. Kondo, H. S. Kato, M. Bonn and M. Kawai, J. Phys. Chem. C **126**, 181103 (2007).

Figure captions

Figure 1

(a) Ps fractions vs incident positron energy for an ASW film grown at 50K at a rate of 6nm min^{-1} on a pre-existing crystalline ice film, for sample temperatures from 50-150K. The mean implantation depth of positrons in a solid of unit density is shown on the upper horizontal axis for guidance only.

(b) Fitted Ps fractions vs sample temperature for the film of Fig. 1(a) (open squares) and for a 700nm-thick film grown on the copper substrate at 50K at a rate of 5 nm/min. (open circles). The open triangles are for the second sample after reducing the temperature from 150K.

Figure 2

(a) $S(E)$ for the 700nm ASW film in Fig. 1(b) at temperatures from 50-150K. S values are normalized to the value for the copper substrate.

(b) Fitted film S values vs temperature for the same sample (black squares). Open circles: S values for the near-surface (80nm thick) layer. The symbols with central crosses are data taken as the temperature was decreased from 150K.

Figure 3

$S(E)$-$W(E)$ plots for the 700nm film of Fig. 2 at T from 50-150K. The large circles represent 'pure annihilation states': Cu = copper, A = ASW film: S = the film surface: C = crystalline ice. The 90 and 110K points are solid to highlight the structural change in the near-surface region.

Figure 4

Film S vs T for four films grown at 50K for the 700nm film (circles), and for μm films grown on crystalline ice at 6nm/min. (squares), on copper at 7nm/min (triangles), and on copper at 200nm/min (diamonds).

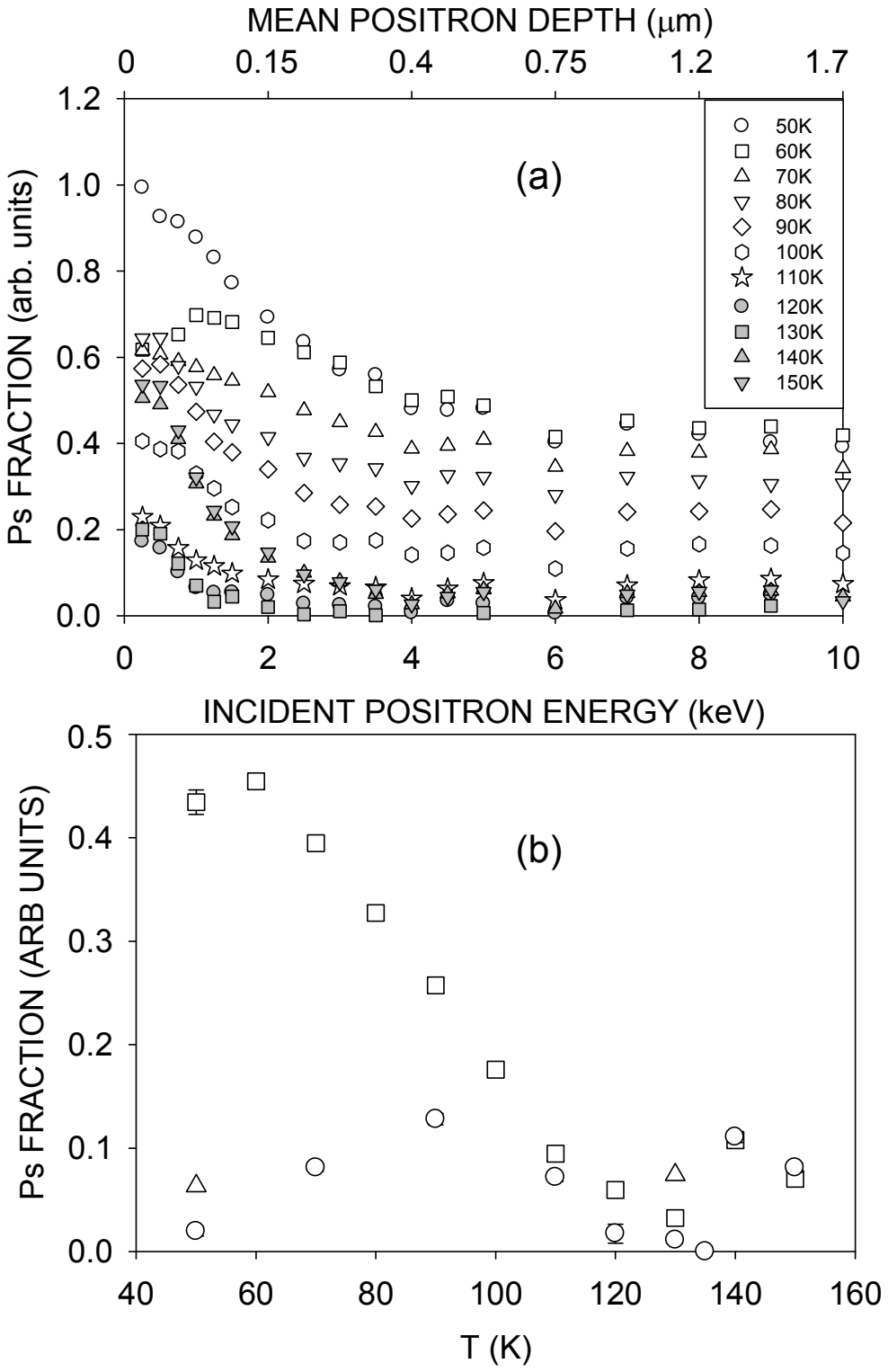
MEAN POSITRON DEPTH (μm)
0
0.15
0.4
0.75
1.2
1.7
Ps FRACTION (arb. units)
(a)
50K
60K
70K
80K
90K
100K
110K
120K
130K
140K
150K
INCIDENT POSITRON ENERGY (keV)
Ps FRACTION (ARB UNITS)
(b)
T (K)

Figure 1

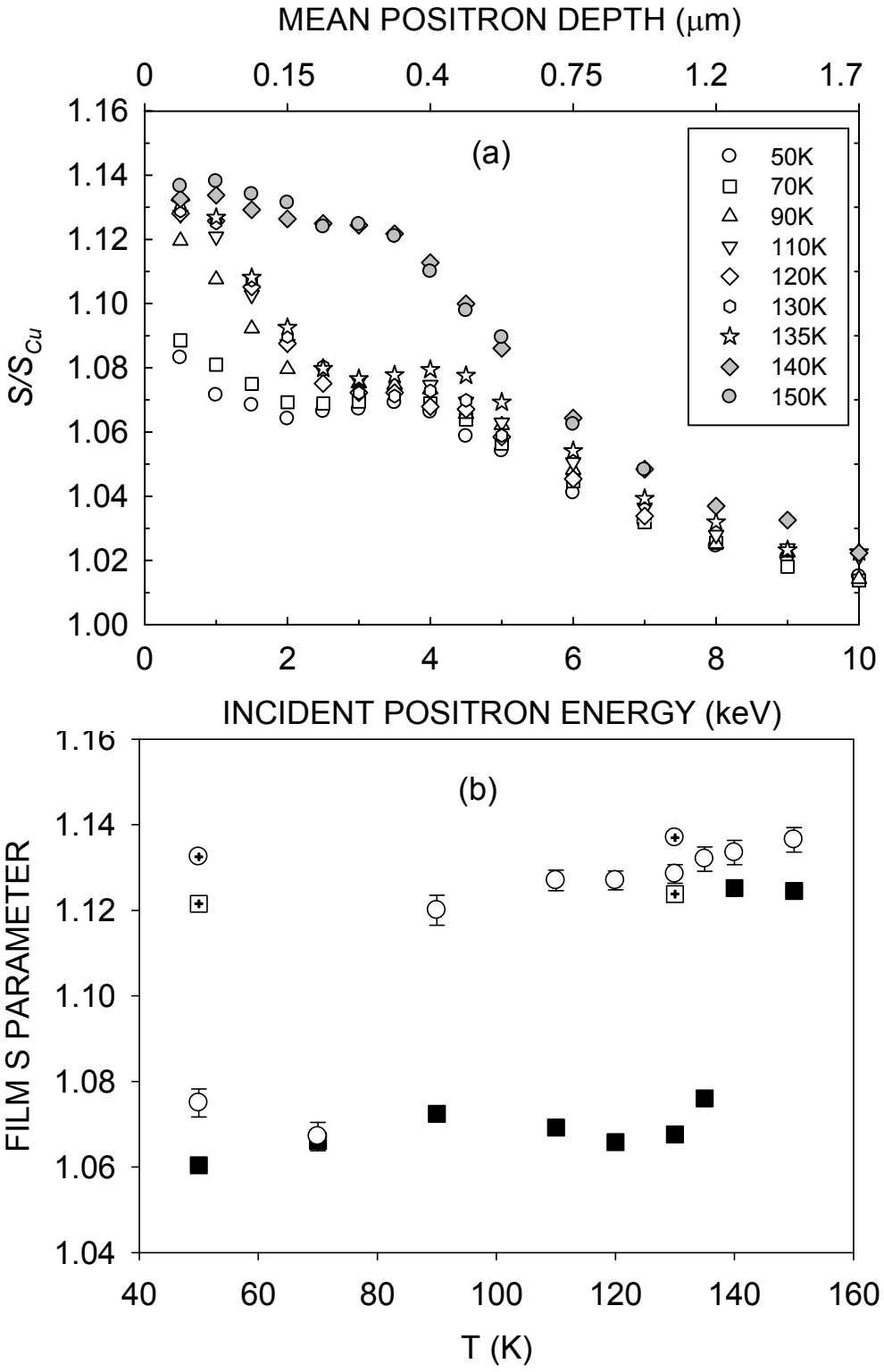
MEAN POSITRON DEPTH (μm)
0
0.15
0.4
0.75
1.2
1.7
(a)
50K
70K
90K
110K
120K
130K
135K
140K
150K
S/S_Cu
1.16
1.14
1.12
1.10
1.08
1.06
1.04
1.02
1.00
0
2
4
6
8
10
INCIDENT POSITRON ENERGY (keV)
(b)
FILM S PARAMETER
1.16
1.14
1.12
1.10
1.08
1.06
1.04
40
60
80
100
120
140
160
T (K)

Figure 2

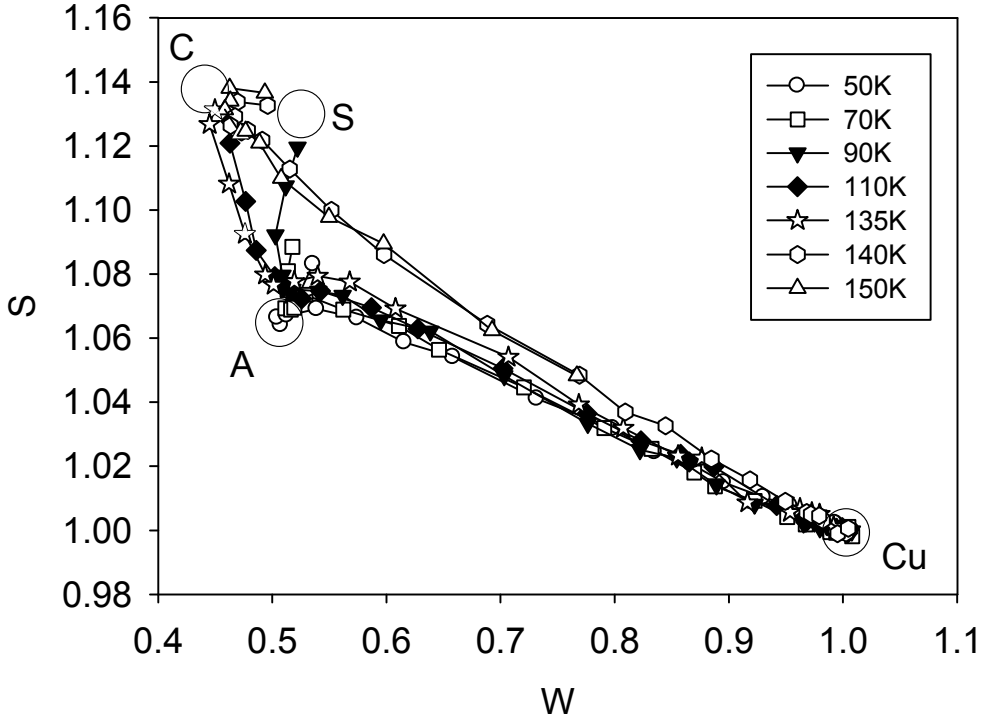
1.16
1.14
1.12
1.10
1.08
1.06
1.04
1.02
1.00
0.98
S
0.4
0.5
0.6
0.7
0.8
0.9
1.0
1.1
W
C
S
A
Cu
50K
70K
90K
110K
135K
140K
150K

Figure 3

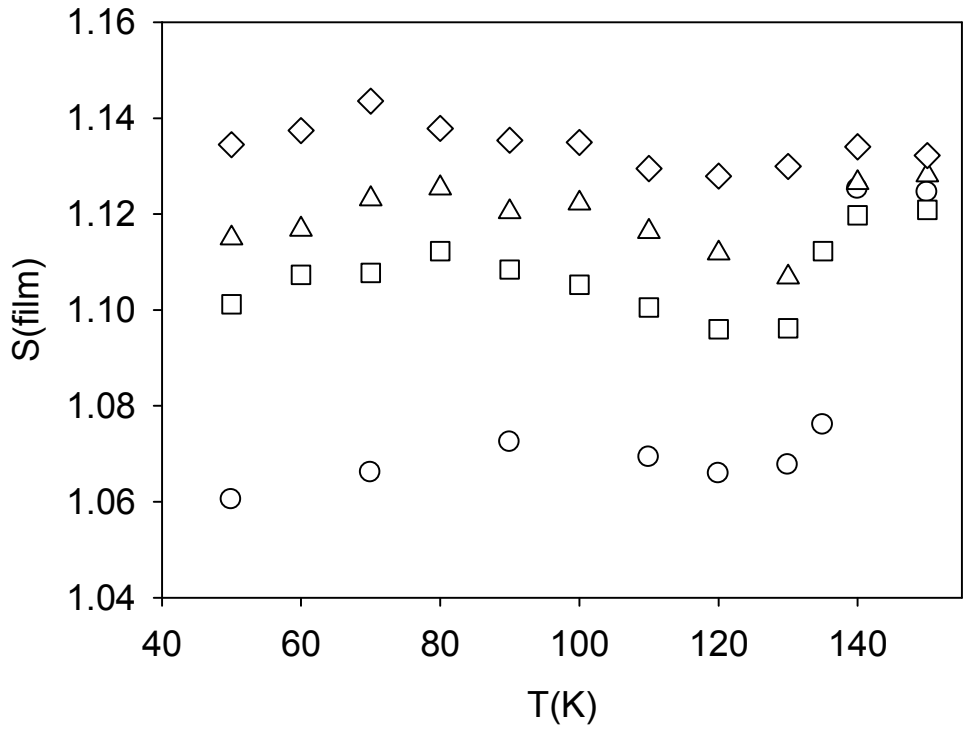

Figure 4